Distributions of Calcium in A and I Bands of Skinned Vertebrate Muscle Fibers Stretched to Beyond Filament Overlap

Marie E. Cantino,* Joseph G. Eichen,# and Stephen B. Daniels*
*Department of Physiology and Neurobiology, University of Connecticut, Storrs, Connecticut 06269 and #Sloan-Kettering Research Center, New York, New York 10024 USA

ABSTRACT Measurements were made of the distributions of total calcium along the length of A and I bands in skinned frog semitendinosus muscles using electron probe x-ray microanalysis. Since calcium in the water space was kept below the detection limit of the technique, the signal was assumed to reflect the distribution of calcium bound to myofilament proteins. Data from sarcomeres with overlap between thick and thin filaments showed enhancement of calcium in this region, as previously demonstrated in rabbit psoas muscle fibers in rigor (Cantino, M. E., T. S. Allen, and A. M. Gordon. 1993. Subsarcomeric distribution of calcium in demembranated fibers of rabbit psoas muscle. *Biophys. J.* 64:211–222). Such enhancement could arise from intrinsic non-uniformities in calcium binding to either thick or thin filaments or from enhancement of calcium binding to either filament by rigor cross-bridge attachment. To test for intrinsic variations in calcium binding, calcium distributions were determined in fibers stretched to beyond filament overlap. Calcium binding was found to be relatively uniform along both thick and thin filaments, and therefore cannot account for the increased calcium observed in the overlap region. From these results it can be concluded that the observed enhancement of calcium is due to an increase in calcium binding to myofilaments as a result of rigor attachment of cross-bridges to actin. The source of the enhancement is most likely an increase in calcium binding to troponin, although enhancement of calcium binding to myosin light chains cannot be ruled out.

INTRODUCTION

Elevation of myoplasmic free Ca^{2+} followed by binding of calcium to troponin leads to the contractile event in vertebrate striated muscle. While troponin has generally been considered to be the primary Ca^{2+}-sensitive switch regulating actomyosin interaction in striated muscle (Ebashi and Endo, 1968), calcium binding to troponin itself appears to be modulated by actomyosin interaction. Such an effect would be expected to result in variations in calcium binding to thin filaments along their length, with more calcium binding occurring in the overlap region of the sarcomere. A number of studies show sarcomere length dependence of ^{45}Ca binding in whole fibers and reconstituted actomyosin preparations under various conditions (see Discussion) and provide evidence that cooperativity in force development depends, at least in part, on cross-bridge attachments. In a previous paper we used electron probe x-ray microanalysis (EPXMA) to make direct measurements of calcium distributions within the sarcomeres of skinned rabbit psoas muscle fibers (Cantino et al., 1993). We showed that calcium was elevated in the region of overlap at all levels of pCa measured, but that the difference was most pronounced at submaximal levels. An important question that could not be resolved in our earlier study was whether there might be an intrinsic elevation in calcium near the ends of either the thick or the thin filaments that could give rise to the observed result. Such variations in calcium might arise from changes in TnC affinity along the length of the thin filament (Gulati, 1993) or variations in calcium binding to myosin light chains along the thick filament. To resolve this question we have made measurements of calcium distributions along the length of A and I bands in fibers stretched to beyond filament overlap, then frozen in rigor solutions with pCa levels varying from 4.5 to 9. Our results show uniform calcium levels along the lengths of both thin and thick filaments in the absence of filament overlap.

MATERIALS AND METHODS

Preparation of glycerinated fiber bundles

Semitendinosus muscles from frogs (*Rana pipiens*) were removed in Ringer's solution (in mM, 95 NaCl; 2.5 KCl; 1.0 $MgSO_4$; 25 $NaHCO_3$; 1.8 $CaCl_2$; 1.0 Na_2HPO_4; 5 glucose, pH 7.3). After pinning and splaying the dorsal head of the muscle, the Ringer's solution was replaced with cold relaxing solution (see Table 1) diluted 50:50 v/v with glycerol. The fibers were then stored for 2–12 days at −16°C. Following storage, small bundles of 8–12 fibers were dissected and skinned in relaxing solution containing 0.6% w/w CHAPS (3-[(3-cholamidopropyl)dimethylammonio]-1-propanesulfonate) for 45 min on ice, with gentle agitation, and then returned to the standard relaxing solution.

Stretching and freezing of fiber bundles

Attachment and freezing of fiber bundles was similar to that described in a previous paper (Cantino et al., 1993), and is summarized here. Following treatment with CHAPS, fiber bundles were transferred to a transducer setup, where they were attached, by wrapping, to a force transducer at one end and to a mechanical stage at the other. The force transducer was a photoelectric displacement measuring device modified after Chiu (Chiu et

Received for publication 3 November 1997 and in final form 17 May 1998.
Address reprint requests to Dr. Marie E. Cantino, Department of Physiology and Neurobiology, University of Connecticut, U-131 Room 129, Beach Hall, Storrs, Connecticut 06269-2131. Tel.: 860-486-3588; Fax: 860-486-1936; E-mail: cantino@oracle.pnb.uconn.edu.

0006-3495/98/08/948/09 $2.00

TABLE 1 Solution composition

Solution	NaP*	Na_2EGTA	MOPS	Na_2ATP	MgP_2 Total	MgP_2 Free	Calcium Total[§] (μM)
Relaxing	100.0[#]	5[#]	10.0	4.0	9.0	4.5	—
Rigor, pCa							
10.00	27.6	13.0	185.0	—	1.4	1.0	2.9
8.98	27.6	13.0	185.0	—	1.4	1.0	33.4
6.07	38.9	0.048	255.0	—	1.0	1.0	33.4
5.71	41.8	0.037	255.0	—	1.0	1.0	33.7
5.21	44.3	0.027	255.0	—	1.0	1.0	31.7
4.55	44.7	0.005	255.0	—	1.0	1.0	32.9

Concentrations in mM, except as noted.
*P, propionate ion.
[#]Contains potassium instead of sodium as the counterion for propionate or EGTA.
[§]As measured by AAS. Includes CaP and contaminating calcium from other sources.

al., 1982). Once attached to the apparatus, the fiber bundles were immersed in a series of Plexiglas wells containing bathing solutions (Hellam and Podolsky, 1969). Fibers were stretched in relaxing solution (see Table 1) to sarcomere lengths of either 3.2 or 3.8 μm, as measured by laser diffraction. Once stretched, fibers were transferred to a pCa 8.98 rigor solution for 15–20 min, then to the final designated pCa rigor solution for another 20 min. The bundle was then raised out of the bath, and clamped with copper clad pliers cooled to liquid nitrogen temperature. Time between removal from the pool and freezing was ~5 s. Frozen fibers were stored in liquid nitrogen until they were cryosectioned.

Solution composition

As in the previous study, two modifications were made to the usual bathing solutions for glycerinated fibers in order to improve calcium detection and to reduce ambiguity of EPXMA data (Kitazawa et al., 1982). First, the final bathing solutions contained Na^+ as the major cation to minimize any error associated with incomplete separation of the potassium K_β and calcium K_α x-ray peaks. The Ca^{2+}-dependence of tension development and the maximal isometric tension of fibers bathed in solutions with Na^+ as the major cation do not differ from those of fibers bathed in solutions with K^+ as the major cation (Gordon et al., 1973; Fink et al., 1986). Second, since EPXMA measures total calcium (bound plus free), the total calcium in solution was kept low and relatively constant (30–36 μM, except in the pCa 10 solution). This level of calcium would contribute a maximum of 0.20 mmol/kg dry wt in a dry cryosection (assuming 85% hydration in the I band before drying) which is at or below the threshold for detection of calcium by EPXMA with our equipment (~0.3 mmol/kg dry wt). Rigor solutions with differing free Ca^{2+} concentrations were prepared by varying the total EGTA concentration. Solution makeup was calculated using the SPECS computer program (Fabiato, 1988), taking into account the binding constant of EGTA for the various constituent ions, corrected for pH, temperature, and ionic strength. Calcium-electrode measurements of calcium propionate and calcium titrated Na_2EGTA stock solutions were used to verify stock concentrations before solutions were mixed. Ionic strength was kept relatively constant, ranging from 146 to 152 mM in the rigor solutions. Total sodium, after titration with NaOH, ranged from 124 to 142 mM. Once pCa solutions (nominally, pCa 9, 6, 5, and 4.5) were made they were assayed by flame atomic absorption spectrophotometry with an acetylene/nitrous oxide flame to determine actual total calcium in solution (contaminating calcium in our solutions is usually found to be 2–4 μM of 32 μM, total). Values were reentered into the SPECS program and revised pCa values computed based on actual total calcium. A correction was also made to correct for ~0.8 μM EGTA that was transferred to the final bath from the pCa 9.0 rigor solution. Solutions having intermediate pCa levels were mixed from the above. Table 1 shows the composition of relaxing and final freezing solutions used (excluding NaOH or KOH used to titrate to pH 7.0).

Preparation of freeze-dried cryosections

Frozen sections were cut in an RMC MT7 with CR-21 cryoattachment. Frozen fibers were mounted on metal chucks with a low temperature glue (s-butyl benzene at −113°C), and sections were cut at −122°C with glass knives at clearance angles of 7°. Dry-cut sections were transferred to formvar and carbon-coated folding grids with an eyelash probe, and were pressed between the two halves of the folded grid with a cold metal rod. The closed grids were freeze-dried by placing them in a cryopumped vacuum chamber on a thermally isolated brass cup cooled to liquid nitrogen temperature. The cup was allowed to warm slowly in the vacuum chamber for a period of 14 h, after which the temperature was raised to slightly above ambient, and samples were moved to a desiccator. Samples were stored over desiccant (aluminum silicate and silica gel) before analysis.

Spectral collection and processing

The principles behind the technique of EPXMA have been described in detail elsewhere (e.g., Hall, 1971; Johnson and Cantino, 1986; LeFurgey et al., 1988; Somlyo et al., 1989). Only those details pertaining to this study will be described. Data were collected in scanning transmission mode in a Zeiss EM910 microscope equipped with an Oxford 30 mm^2 Si(Li) x-ray detector and an Oxford ExLII analytical system. As in our previous study, two modes of data collection were used. Digital x-ray images were acquired by positioning the beam in a 128 × 128 pixel array for 4–8 s per pixel, a process requiring 18–36 h per image. Data from two to four such images were combined to produce calcium and mass distributions from only a few sarcomeres, but at high spatial resolution. Alternatively, in "analog raster" analysis, the beam was scanned in a rectangular raster for 1000 s to obtain average calcium concentrations over approximately one-third of each A or I band in four to five sarcomeres from each fiber. In this mode, a larger number of fibers could be sampled at lower resolution to verify that the image data (above) were obtained on fibers that were representative in terms of the average concentration of calcium present on the filaments.

Analog raster and image analysis were carried out at room temperature using a side entry goniometer stage tilted 20° toward the detector. A scan rotation device allowed orientation of the rectangular raster relative to the ultrastructure. The grid was oriented so that the fiber axis was parallel to the tilt axis of the stage to eliminate mixing of adjacent regions of analysis within the sarcomere when the stage was tilted. The diameter of the beam was estimated (based on measurements of the transmitted beam and on edge profiles from x-ray images of an aluminum film) to be 100 nm, with specimen currents of 10–20 nA. For analog raster analysis, rectangular rasters were ~0.2 × 1.0 μm, and were oriented with their long axes perpendicular to the fiber axis so that they spanned the entire width of the sarcomere. Support film spectra or images were collected immediately adjacent to the section and were used to estimate the magnitude of corrections for both continuum and calcium x-ray counts contributed by the support film to each myofilament spectrum. Measurements of beam current at the specimen were used to adjust film corrections for any differences in total dose in each spectrum or at each pixel.

Spectra were processed using digital filtering and linear least-squares fitting programs (Shuman et al., 1976) resident on the Oxford ExLII and described previously (Cantino et al., 1993). These routines yielded peak and bremstrahlung (1.34–1.64 keV) integrals for the unknown spectrum. Dry weight concentrations for calcium were computed by normalizing the film corrected peak counts to the film corrected bremstrahlung counts and multiplying by proportionality constants determined from protein and binary standards, with corrections for the difference in the average atomic number of the standard and that of the unknown. Since standards are collected under low dose conditions, corrections for beam-induced loss of the hydrocarbon matrix in the sections were made based on separate low

and high dose measurements of bremstrahlung in freeze-dried cryosections. These were applied after quantitation.

Digital x-ray and scanning transmission electron microscopy (STEM) images were collected simultaneously at room temperature in 128 × 128 × 16 bit arrays with dwell times of 4–8 s per pixel. Drift correction software (Statham, 1987) was used to correct for specimen drift during acquisition. Spectral analysis used to obtain characteristic and bremstrahlung x-ray intensities at each pixel was the same as that described above. Image data were transferred to an Apple Power Mac 7100 and imported into the IPLAB spectrum image analysis package (version 3.1a; Signal Analytics Corp., Vienna, VA). Profiles corresponding to calcium or bremstrahlung (mass) distributions along A and I bands were generated using procedures summarized in Fig. 1. The STEM images (Fig. 1 *A*) were used to define "masks" aligned to the sarcomere structure; since x-ray and electron images are acquired simultaneously, there can be no misalignment between images. Masks were drawn at the left Z line, one edge of the A band, and the right Z line to derive data from, respectively, the left I band, the A band, and the right I band. Pixels corresponding to remnants of sarcoplasmic reticulum (SR) or mitochondria were identified from the P image (Fig. 1 *B*) and corresponding pixels in the targeted x-ray image (for example, the bremstrahlung or "mass" image shown in Fig. 1 *C*) were set to zero to eliminate their contribution to counts within that image. Each mask was then applied to the targeted x-ray image and translated horizontally, pixel by pixel, across the image. At each horizontal position, the sum of all pixel values was computed to generate a single "mask sum." The combination of all such sums produced a one-dimensional array representing the total x-ray intensity distribution across the sarcomeres sampled (Fig. 1 *D*). The same procedure was applied to the calcium image. Since calcium distributions were assumed to be symmetrical around the center of the sarcomere, we improved signal-to-noise ratios by treating data from left- and right-half sarcomeres in the same image as separate data sets. Thus, left- and right-half sarcomere arrays from the same image were aligned at the Z line, while A band arrays were split and aligned at the center. These were combined with similar half-sarcomere arrays from other images. Thus, data in Figs. 5 and 6 represent means and standard errors of the mean over all half-sarcomere arrays.

Arrays of calcium and bremstrahlung counts, once obtained as described above, were transferred to a spreadsheet where corrections were made for contributions of the film. Film corrected count data were then treated in one of two ways. For concentration profiles, a ratio of the calcium mask sum to the bremstrahlung mask sum was computed for each mask and expressed as a concentration in mmol/kg dry wt. These values are useful in areas where protein distributions are uniform, since they can be compared to values predicted by other methods. However, in areas where mass is contributed by additional proteins (such as in the overlap region and the Z line), concentration data will reflect both variations in calcium per troponin as well as variations in total mass. In these cases it is also instructive to examine the distribution of counts. Count distributions reflect the calcium bound per unit distance along the sarcomere, provided that the filament density, section thickness, and beam conditions are constant within each half-sarcomere-long row of pixels. Constancy of beam current (within a percent) has been verified with a Faraday cup. Constancy of section thickness within a particular field is confirmed by the similarity of bremstrahlung intensities in each half of profiles such as shown in Fig. 1 *D*. Filament density was examined by measuring the myofibrillar diameter in conventional thin sections. It was found to increase only slightly (average, 6%) in the overlap region of sarcomeres at 3 to 3.3 μm. This increase will tend to underestimate the degree of enhancement of calcium binding by 10–15% by decreasing the number of thin filaments in the overlap region (e.g., in Fig. 3).

Although counts reflect variations in calcium binding per unit distance within each profile, the absolute intensity of profiles depends on section thickness, mask width, and electron dose (beam current and dwell time). To remove these map-to-map variables, all calcium mask sums in each half-sarcomere profile were normalized to a single scaling factor: the average bremstrahlung for all mask sums in that half-sarcomere, which depends on the same factors. When profiles from images acquired on different days and from different sections are statistically pooled, the variance then reflects primarily counting statistics and intrinsic sarcomere-to-sarcomere variation.

Conventional preparation of semitendinosus muscle for electron microscopy

Bundles of semitendinosus muscle, skinned, mounted, and stretched as above, were transferred to a fixative containing 0.1 M Hepes buffer, 1.5% glutaraldehyde, and 1.5% formaldehyde, pH 7.3. Samples were post-fixed in 2% OsO_4 (in 0.1 M Hepes) then were dehydrated through a graded ethanol series and embedded in an epoxy (SPIpon-Araldite) resin. Sections were post-stained in uranyl acetate and lead citrate, and were examined in a Phillips 300 electron microscope at 80 kV.

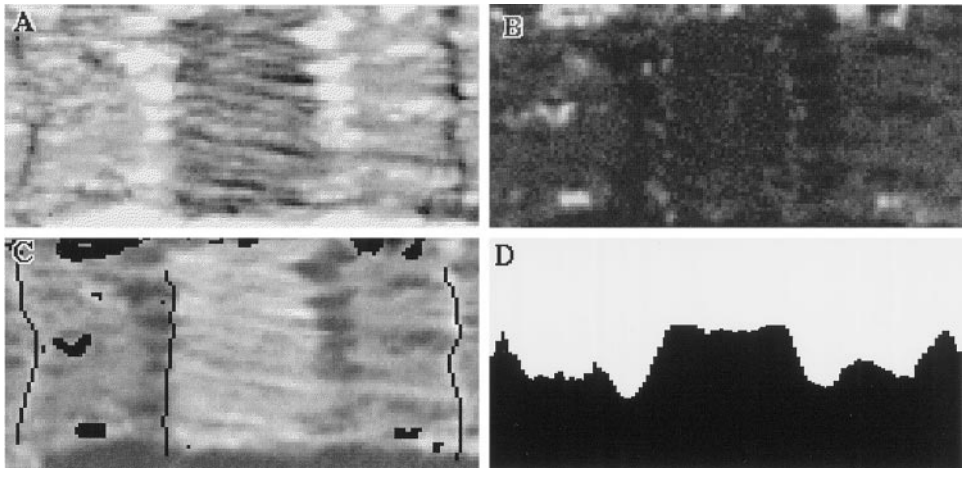

FIGURE 1 Digital image analysis procedures used in this study. (*A*) The STEM image of sarcomeres in the image field is used to identify positions of A and I bands in the sarcomere (fiber frozen at pCa 5.2). (*B*) The P image is used to identify putative membrane fragments from SR and mitochondria. (*C*) The high P pixels selected from the P image are zeroed in the x-ray image to be analyzed; in this case, the bremstrahlung image shows the distribution of mass in the sample. Masks following the contours of each Z line and the edge of the A band are shown overlaid (*in black*) on the corrected bremstrahlung image. Each of these masks is translated across the image to select a region of interest in which all counts are summed. (*D*) The resulting intensity distribution represents total bremstrahlung signal as a function of position across the image.

RESULTS

Calcium-binding enhancement in the overlap region of frog fast twitch fibers

Our earlier data showing enhancement of calcium binding in the overlap region (Cantino et al., 1993) were collected from skinned rabbit psoas muscle; however, our initial attempts to produce well-aligned sarcomeres in muscles stretched to beyond filament overlap were unsuccessful. Sarcomeres in these fibers tended to undergo severe skew and misalignment at long lengths, making identification of A-band and I-band regions in cryosections nearly impossible. This phenomenon was reported previously in rabbit psoas muscle by Carlsen and co-workers (Carlsen et al., 1965a, b).

To provide the best possible filament alignment, we chose instead to use frog semitendinosus muscle, which can be stretched to long lengths with relatively little misalignment of filaments. Since ultrastructure in the freeze-dried cryosections is sometimes difficult to interpret, we prepared ultrathin sections of overstretched muscle using our initial isolation, stretching, and rigorization protocol, followed by conventional embedding. An example is shown in Fig. 2. Although sarcomere length in these fibers vary, many sarcomeres are clearly stretched to beyond filament overlap and show a well-defined gap between the ends of the thin and beginning of the thick filaments (never clearly visible in the rabbit psoas muscles).

Before proceeding with experiments involving long lengths, we first investigated whether enhanced calcium levels are observed in the overlap region of frog semitendinosus sarcomeres, as we previously found in rabbit psoas muscle. Fig. 3 shows calcium (*A*) and bremstrahlung (*B*) distributions from a fiber frozen at pCa 5.7 relative to the A, I, and overlap regions of the sarcomeres (*C*). Data at each point represent the mean ± SE of x-ray counts from eight profiles. Numbers below the calcium distribution in Fig. 3 *A* represent mean ± SD of all points between the arrowheads. Substantially more calcium is present in the overlap region than would be expected from the sum of H-zone and I-band calcium, consistent with previous measurements from rabbit psoas muscle (Cantino et al., 1993). The calcium and bremstrahlung distributions fall off at the same position along the sarcomere, indicating that enhancement of calcium binding does not extend more than a few regulatory units into the thin filament. This is also consistent with previous observations in rabbit muscle.

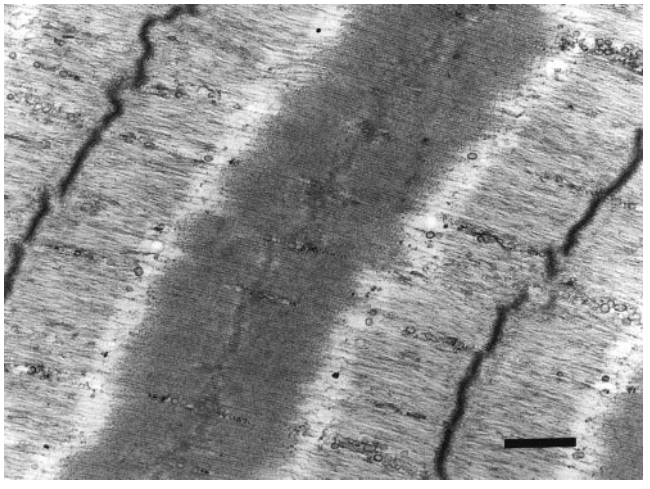

FIGURE 2 A conventionally fixed and embedded thin section of a sample of overstretched frog semitendinosus muscle shows good alignment of the myofilaments, although some irregularity occurs. Comparison with Fig. 1 *A* shows that some further disruption of the myofilament lattice occurs during freezing and sectioning, but that overall the structure is comparable. Bar = 0.5 μm.

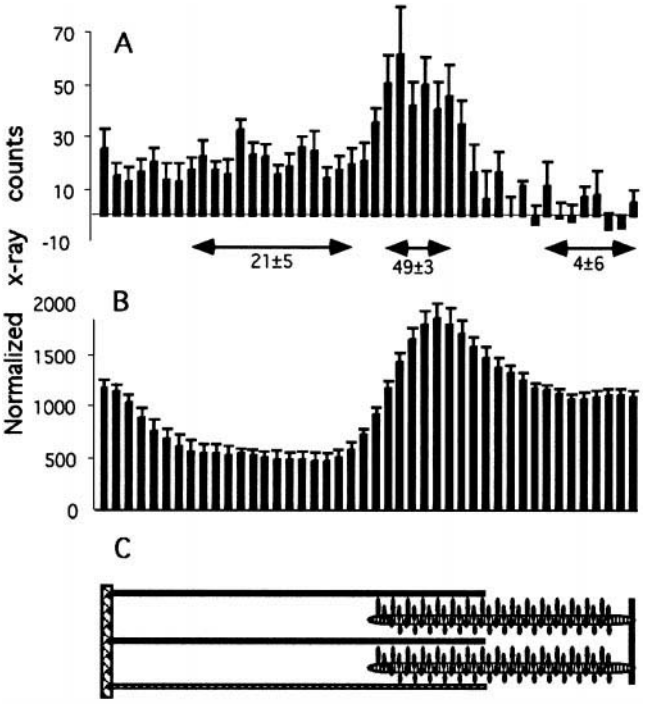

FIGURE 3 Normalized x-ray count profiles from (*A*) the calcium image and (*B*) the bremstrahlung image of a frog semitendinosus fiber frozen at ~3.2 μm sarcomere length. The x-ray count distributions are aligned relative to the corresponding sarcomere structure as shown in (*C*).

Calcium distributions in A and I bands of overstretched frog muscle fibers

To test whether this elevation in calcium binding is due to intrinsic variations in the amount of calcium bound to the myofilaments, we examined fibers stretched to 3.4 μm or above, then placed into rigor solutions at various pCa levels. Three fibers from each of five separate pCa levels were analyzed to determine calcium concentrations in the non-overlap A and I bands using static raster analysis. Results are plotted in Fig. 4. Calcium levels in the I band rise dramatically as the free Ca^{2+} is raised from pCa 8.98 to 6.07, presumably corresponding primarily to the binding of calcium to high-affinity sites on TnC. A further increase is

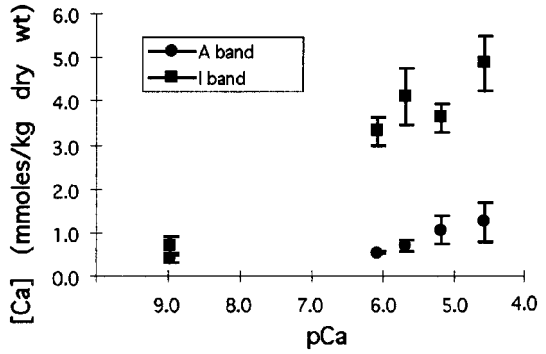

FIGURE 4 Concentrations of calcium measured with static rasters placed in A and I bands of frog semitendinosus fibers at five different free calcium concentrations.

TABLE 2 Dry mass concentrations of sodium and potassium from static raster analyses

Region	pCa	Sodium	Potassium	*N* Fibers (Spectra)
I band				
	8.98	1063 ± 38	2.6 ± 1.8	3 (15)
	6.07	918 ± 204	1.5 ± 0.6	3 (15)
	5.71	1176 ± 47	1.2 ± 0.1	3 (15)
	5.21	1242 ± 24	1.1 ± 0.1	3 (15)
	4.55	1147 ± 79	1.7 ± 0.6	3 (15)
A band				
	8.98	712 ± 56	1.0 ± 0.3	3 (15)
	6.07	647 ± 77	1.4 ± 0.5	3 (15)
	5.71	831 ± 89	1.0 ± 0.2	3 (15)
	5.21	817 ± 46	0.8 ± 0.2	3 (15)
	4.55	784 ± 81	1.2 ± 0.3	3 (15)

Results are in mmol/kg dry wt (mean ± SE for *N* fibers).

observed when free Ca^{2+} is raised from pCa 6.07 to 4.55. In contrast, A-band calcium shows little increase from 8.98 to 6.07, but rises substantially at pCa 5 and above. Similar increases in calcium binding to TnC have been shown previously with EPXMA (Kitazawa et al., 1982; Cantino et al., 1993), although maximal binding at pCa 4.5 is somewhat lower than expected if all four TnC sites are saturated with calcium.

To test whether the low concentration of calcium detected in the I band at pCa 8.98 (see Fig. 4) arises from calcium bound to EGTA in the water space, we also froze and analyzed one fiber in a solution containing only 3 μM total calcium (see Table 1, pCa 10.0). Calcium in the I bands of this fiber measured 0.6 ± 0.2 mmol/kg dry wt, (mean ± SE for five spectra), similar to the 0.7 mmol/kg dry wt measured in fibers frozen in solutions containing 33 μM total calcium. This supports our assumption that the calcium in the solution space between the myofilaments is not detectable in freeze-dried cryosections. We have not determined whether this residual calcium signal is due to a slowly exchanging bound pool of calcium remaining in the myofibrils or to some small systematic error in our quantitation procedure.

We also examined the concentrations of sodium and potassium in EPXMA spectra. As seen in Table 2, the concentration of sodium was nearly three orders of magnitude higher than that of potassium, which was close to zero. While rigor solutions contained 124 to 142 mM total sodium, this cation was replaced with a similar amount of potassium in the relaxing solutions. Therefore, this difference in the EPXMA spectra confirms that the relaxing solution was washed out before freezing.

From these fibers we chose samples with regions stretched to 3.6 μm or beyond and having the best alignment of sarcomeres, and used them to collect higher-resolution data using digital image acquisition. In Fig. 5, *A–D* are calcium concentration distributions from both A and I bands at several pCa levels. Since magnifications varied from map to map, the horizontal axes of distributions in Fig. 5, *A–D* have been scaled so that all have the same A and I band length, allowing for easier comparison to the sarcomere structure as represented schematically in *E*. These concentrations obtained from images are generally comparable to data in Fig. 4 acquired with static raster analysis. Distributions for pCa 9.0 to 5.2 show relatively constant calcium concentrations along the length of both thick and thin filaments, except near the Z line.

To determine whether the drop in calcium concentration near the Z line is due to changes in calcium per unit length of filament or due to addition of (non-calcium binding) mass in this area, we also examined normalized count distributions (see Methods), shown in Fig. 6, *A–D*. Note that the calcium remains level all the way to the Z line, consistent with the hypothesis that calcium binding to troponin is uniform, and that the drop seen in Fig. 5 is due to increased mass from the Z line. The count distributions also serve to rule out the possibility that calcium binding along the filaments actually increases, but that this increase is masked by a comparable increase in the mass due to some added mass component such as titin. No such increase is seen, although there is a slight decline in calcium at the tips of thick and thin filaments at pCa 4.6.

Because static raster analysis does not permit selected removal of high P areas from the region of analysis, we used high P regions removed from images to assess the possible effect of inclusion of these areas in the static raster analysis. Mean calcium concentrations in high P pixels removed from images are shown in Fig. 7 for the four levels of pCa examined using x-ray image data. While calcium levels in these pixels do increase with decreasing pCa they are, in all cases, the same or lower than the those levels in the I band, but are, at pCa 6 and above, substantially higher than A band concentrations (see Fig. 4).

DISCUSSION

There is now substantial evidence that calcium binding to TnC is enhanced in the region of overlap between thick and thin filaments. Modulation of ^{45}Ca binding to troponin by cross-bridge attachment has been reported by a number of

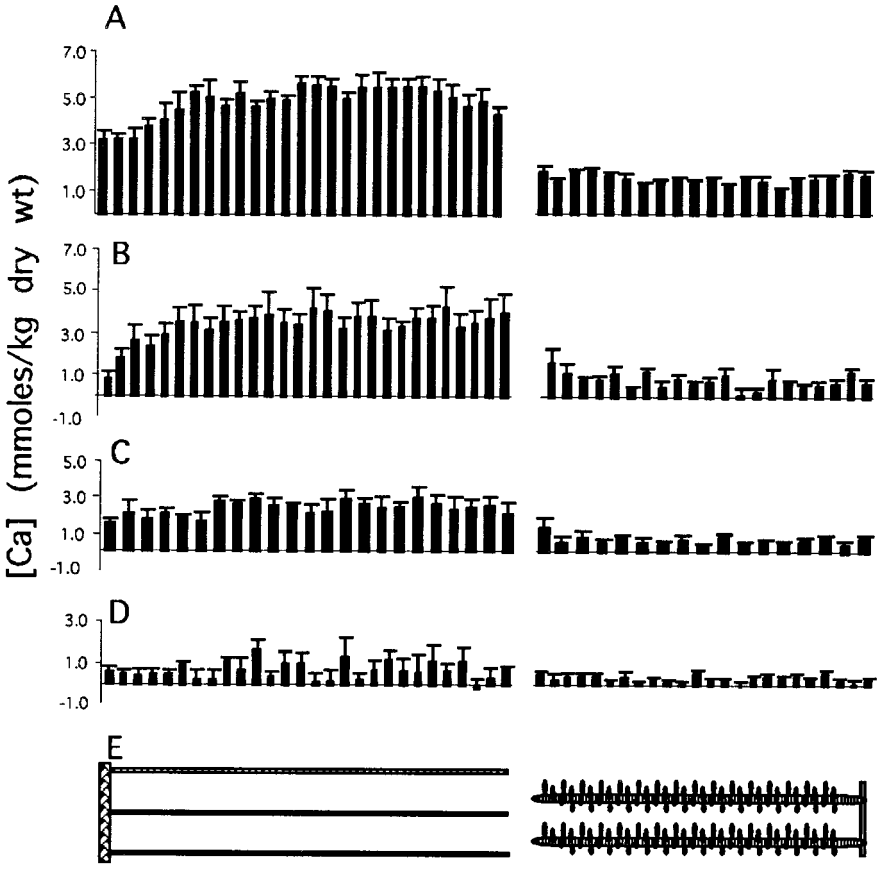

FIGURE 5 Calcium concentration profiles across A and I bands from images of fibers frozen at various free calcium concentrations: (*A*) pCa 4.6 (mean ± SE for four profiles); (*B*) pCa 5.2 (mean ± SE for six profiles); (*C*) pCa 6.1 (mean ± SE for four I-band and seven A-band profiles); (*D*) pCa 9.0 (mean ± SE for six profiles). Alignment of I band (*left*) and A band (*right*) relative to the profiles is shown in (*E*).

investigators (Bremel and Weber, 1972; Fuchs, 1977a, b; Pan and Solaro, 1987; Hofmann and Fuchs, 1987) in various states and muscle types. Studies using fluorescent labeled TnC incorporated into skeletal muscle fibers provide evidence that rigor cross-bridge formation produces structural changes in the vicinity of the probe, providing a mechanism for alterations in calcium binding (Trybus and Taylor, 1980; Guth and Potter, 1987; Gordon et al., 1988; Allen et al., 1992). Further support for cross-bridge effects can be found in aequorin studies of changes in myoplasmic free Ca^{2+} following length changes in barnacle skeletal fibers (Ridgway and Gordon, 1984) and mammalian ventricular muscle (Allen and Kurihara, 1982). These researchers proposed that sudden detachment of cross-bridges leads to increased myoplasmic free Ca^{2+} and concluded that the detachment of cross-bridges reduces the calcium-affinity of troponin.

Although these studies have provided a firm basis for the hypothesis that cross-bridge attachments act cooperatively to enhance calcium binding to TnC, they do not have the spatial resolution to detect variations in calcium binding along the thin filament. Spatially resolved measurements of calcium binding were first carried out by Winegrad (1965), who found enhanced ^{45}Ca levels in the overlap region of muscles fixed for autoradiography. More recently we detected elevated calcium levels in the overlap region of skinned rabbit psoas sarcomeres, using EPXMA (Cantino et al., 1993). We attributed these results to enhanced binding of calcium to TnC resulting from strong cross-bridge attachment; however, these data alone did not allow us to rule out two alternative explanations for the increased binding in the overlap region. First, although we did correct the amount of calcium observed in the overlap region for the contribution by calcium binding to myosin, this correction was based on measurements made toward the center of the H zone. Since the protein composition at the center of the thick filaments changes substantially due to absence of myosin heads and presence of M line proteins, it remained possible that our correction factor underestimated the true magnitude of myosin calcium binding at the ends of the thick filaments, i.e., in the overlap region. This effect, if sufficiently large, could give rise to the observed calcium binding enhancement in our images and static raster data.

A second explanation for the observed results is that calcium binding to the thin filament is non-uniform. This has been proposed as a molecular mechanism for the steep length dependence of calcium sensitivity in cardiac muscle (Gulati, 1993). In this scheme, the affinity of TnC itself is non-uniform along the length of the thin filament, with higher affinity at the free end. This distribution, if it exists, might produce an observed elevation in calcium in the overlap region, unrelated to the attachment of cross-bridges.

Our results on frog semitendinosus muscle in rigor would appear to rule out either of these possibilities, at least in skeletal muscle. As in rabbit psoas muscle, we find substantial enhancement of calcium binding in the overlap region of skinned frog fibers. However, when these fibers are

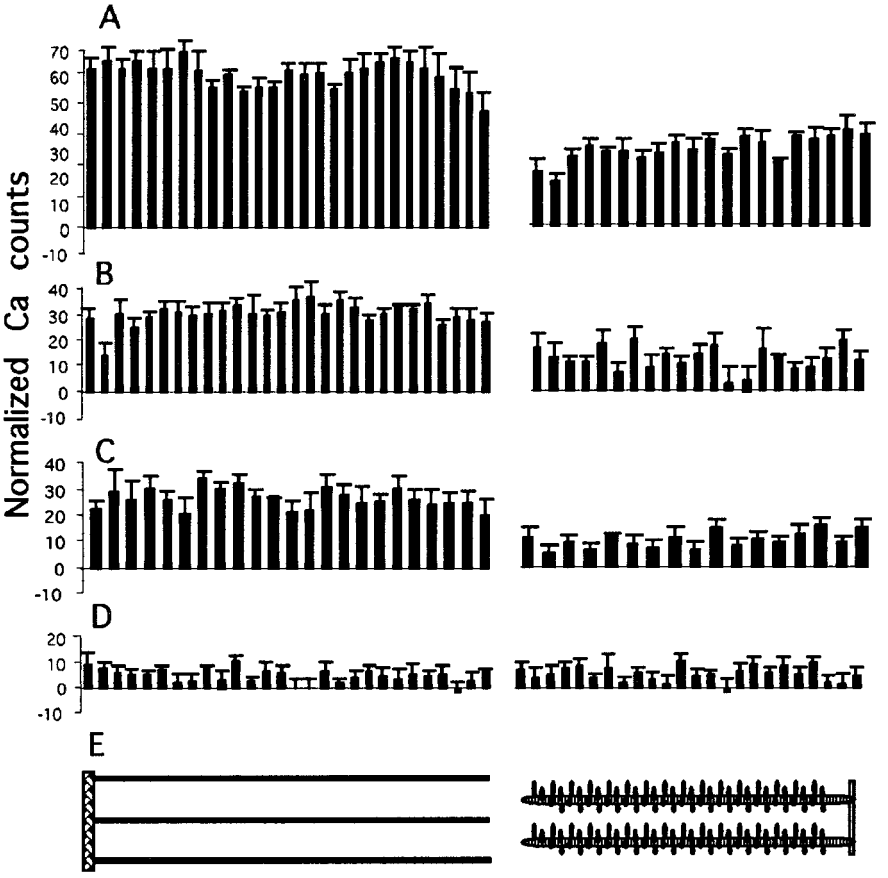

FIGURE 6 Normalized calcium count profiles across A and I bands from images of fibers frozen at various free calcium concentrations. (*A*) pCa 4.6 (mean ± SE for four profiles); (*B*) pCa 5.2 (mean ± SE for six profiles); (*C*) pCa 6.1 (mean ± SE for four I-band and seven A-band profiles); (*D*) pCa 9.0 (mean ± SE for six profiles). Alignment of I band (*left*) and A band (*right*) relative to the profiles is shown in (*E*).

stretched to beyond filament overlap, the calcium distribution measured by EPXMA is uniform over most of the A and I bands. In some cases there appeared to be some decline in calcium levels at the end of the I band (see Fig. 6 *A*). The presence of a similar drop in bremstrahlung profiles (data not shown) suggested that this was primarily related to misalignment of I bands from different parts of the image and from different images; this is reflected in the reduction in this decline when the calcium signal is normalized to the *local* bremstrahlung, as in the concentration profiles in Fig. 5. The variations in filament length observed may arise in part from skewing that is intrinsic to the myofilaments in these sarcomeres, but the majority arose from the necessity of averaging multiple profiles. We found that cryosectioning produced variable compression, which led to variation in I and A band lengths from one field to another. Despite this mitigating factor, it is clear that over at least 80% of the thin-filament calcium levels remain relatively constant. It seems extremely unlikely that calcium binding could increase in the last 20% of the thin filament to sufficient levels to give rise to the 1.5–2-fold enhancement seen in the overlap region.

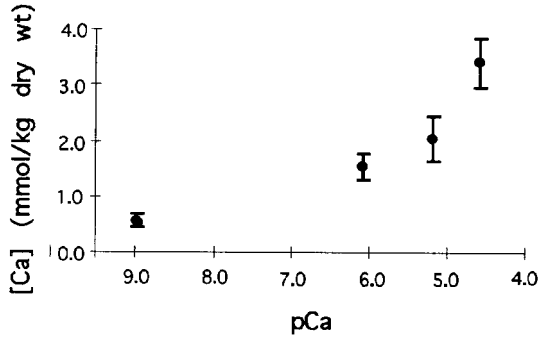

FIGURE 7 Calcium concentrations derived from high P pixels removed before image analysis of subsarcomere distributions shown in Fig. 6. Values are mean ± SE for data from *n* images. Fibers were frozen at pCa: (*A*) 9.0, $n = 4$; (*B*) 6.1, $n = 6$; (*C*) 5.2, $n = 5$; (*D*) 4.6, $n = 4$.

As expected, the amount of calcium measured in the A band is well below that in the I band at levels of pCa between 6.1 and 4.6. Nonetheless, substantial increases in A band calcium concentration occur between pCa 6.1 and 4.6 (Figs. 4 and 5). These increases are likely to be due to binding to myosin light chains, which bind up to two moles of calcium per mole of myosin (Holroyde et al., 1979). If myosin contributed all of the mass in the A band, and all light chain sites were saturated, the concentration of calcium measured by EPXMA would be ~4 mmol/kg dry wt, well above the 1.3 ± 0.5 mmol/kg dry wt measured here. However, in the presence of 1 mM Mg^{2+} it is unlikely that all sites are saturated at pCa 4.6, and other mass-contributing components such as titin, C protein, and M line proteins may reduce the maximum dry weight concentration.

The significance of increases in calcium associated with myosin is unclear, since kinetics of calcium binding to isolated myosin are too slow to contribute to activation (Bennett and Bagshaw, 1986). It is possible that kinetics measured in isolated systems differ from those in the intact sarcomere. While the distributions in Figs. 5 and 6 argue strongly against calcium binding enhancement in the overlap region being a result of intrinsic variations in calcium binding along the thick filament, it remains possible that cross-bridge attachment to actin enhances the affinity of myosin regulatory light chain for calcium, just as it appears to enhance the affinity of TnC for calcium. In this case some portion of the calcium enhancement seen in the overlap region might arise from calcium binding to myosin. Such an effect would be interesting in the light of proposals that calcium binding to myosin RLC increases the number of strongly attached cross-bridges (Moss, 1992).

If calcium measured in the A band is bound primarily to myosin light chains, then it is somewhat surprising that no decrease was detected in calcium at the center of the sarcomere, where no myosin heads are present. The often imperfect alignment of M lines (as evident in Fig. 1) and slight misalignments between profiles in the average would tend to smear out any reduction. A second possibility is that calcium binds to M line proteins, so that any decrease in the bare zone is masked. At pCa 4.5 some elevation of calcium was sometimes seen at the center of the sarcomere; however, this elevation seemed to be associated with elevated P and was largely removed by the correction for high P pixels (see Methods). As indicated in Fig. 7, high P areas have calcium concentrations substantially above A band levels at pCa 4.5. Even in conventional ultrathin sections, regions of membrane fragments are sometimes found at the level of the A band. These regions, if below the threshold for pixel removal, would elevate calcium levels at the center of the sarcomere. Calcium bound to membrane fragments in skinned fibers, if they constitute a large enough fraction of the myofibrillar mass, could also be a significant contribution to total fiber calcium measured by other techniques.

It is now generally accepted that other accessory proteins are present in the I band, notably titin and nebulin. These proteins contribute mass, and possibly calcium, to these measurements. By using existing data on relative mass fractions and distributions of actin, tropomyosin, troponin, titin, and nebulin in the sarcomere we previously estimated that mass contributed by titin and nebulin would lower the contribution of each mole of calcium bound to troponin from 2.25 to 1.7 mmol/kg dry wt in the I band. As previously noted, this is consistent with the levels of 6.8 mmol/kg dry wt seen in overlap regions of rabbit psoas fibers, though above levels seen in the non-overlap I band (Cantino et al., 1993). In the current study, I band levels are closer to what would be predicted for three calcium atoms bound to troponin; however, calcium levels measured in pCa 4.6 fibers were quite variable, with some measurements close to the predicted levels for four binding sites. It is also possible that not all sites are saturated at pCa 4.6. If calcium binding to titin or nebulin occurs in skeletal muscle, EPXMA measurements suggest that it is relatively small in magnitude, and uniform in distribution.

The authors are grateful to James Romanow for constructing the apparatus for mounting and monitoring muscle fibers for these experiments and for his daily efforts to keep the equipment used in this work in full operation. We also thank Dr. Lamia Khairallah for suggestions regarding electron microscopy of embedded samples and Drs. Albert Gordon, Bryant Chase, Donald Martyn, and Robin Mondares for advice in carrying out this work.

This work was supported by National Institutes of Health Grant HL49443 and the University of Connecticut Research Foundation.

REFERENCES

Allen, D. G., and S. Kurihara. 1982. The effects of muscle length on intracellular calcium transients in mammalian cardiac muscle. *J. Physiol.* 327:79–94.

Allen, T. S., L. D. Yates, and A. M. Gordon. 1992. Ca^{2+}-dependence of structural changes in troponin-C in demembranated fibers of rabbit psoas muscle. *Biophys. J.* 61:399–409.

Bennett, A. J., and C. R. Bagshaw. 1986. The kinetics of bivalent metal ion dissociation from myosin subfragments. *Biochem. J.* 233:173–177.

Bremel, R. D., and A. Weber. 1972. Cooperation within actin filament in vertebrate skeletal muscle. *Nature*. 238:97–101.

Cantino, M. E., T. S. Allen, and A. M. Gordon. 1993. Subsarcomeric distribution of calcium in demembranated fibers of rabbit psoas muscle. *Biophys. J.* 64:211–222.

Carlsen, F., F. Fuchs, and G. G. Knappeis. 1965a. Contractility and ultrastructure in glycerol-extracted muscle fibers. The relationship of contractility to sarcomere length. *J. Cell Biol.* 27:25–34.

Carlsen, F., F. Fuchs, and G. G. Knappeis. 1965b. Contractility and ultrastructure in glycerol-extracted muscle fibers. II. Ultrastructure in resting and shortened fibers. *J. Cell Biol.* 27:35–46.

Chiu, Y., J. Asayama, and L. E. Ford. 1982. A sensitive photoelectric force transducer with a resonant frequency of 6 kHz. *Am. J. Physiol.* 243: C299–C302.

Ebashi, S., and M. Endo. 1968. Calcium ion and muscle contraction. *Prog. Biophys. Mol. Biol.* 18:123–183.

Fabiato, A. 1988. Computer programs for calculating total from specified free or free from specified total ionic concentrations in aqueous solutions containing multiple metals and ligands. *Methods Enzymol.* 157: 378–413.

Fink, R. H. A., D. G. Stephenson, and D. A. Williams. 1986. Potassium and ionic strength effects on the isometric force of skinned twitch muscle fibres of the rat and toad. *J. Physiol.* 370:317–337.

Fuchs, F. 1977a. The binding of calcium to glycerinated muscle fibers in rigor, the effect of filament overlap. *Biochim. Biophys. Acta*. 491: 523–531.

Fuchs, F. 1977b. Cooperative interactions between calcium-binding sites on glycerinated muscle fibers. The influence of cross-bridge attachment. *Biochim. Biophys. Acta*. 462:314–322.

Gordon, A. M., R. E. Godt, S. K. B. Donaldson, and C. E. Harris. 1973. Tension in skinned frog muscle fibers in solutions of varying ionic strength and neutral salt composition. *J. Gen. Physiol.* 62:550–574.

Gordon, A. M., E. B. Ridgway, L. D. Yates, and T. Allen. 1988. Muscle cross-bridge attachment: effect on calcium binding and calcium activation. *Adv. Exp. Med. Biol.* 226:89–98.

Gulati, J., editor. 1993. Molecular biology of the length-tension relation in cardiac muscle. *In* Mechanism of Myofilament Sliding in Muscle Contraction. Plenum Press, New York. 593–602.

Guth, K., and J. D. Potter. 1987. Effect of rigor and cycling cross-bridges of the structure of troponin C and on the Ca^{2+} affinity of the Ca^{2+}-specific regulatory sites in skinned rabbit psoas fibers. *J. Biol. Chem.* 262:13627–13635.

Hall, T. A. 1971. The Microprobe Assay of Chemical Elements. Academic Press, New York. 157–261.

Hellam, D. C., and R. J. Podolsky. 1969. Force measurements in skinned muscle fibers. *J. Physiol.* 200:807–819.

Hofmann, P. A., and F. Fuchs. 1987. Effect of length and cross-bridge attachment on Ca^{2+} binding to cardiac tropinic C. *Am. J. Physiol.* 253:C90–C96.

Holroyde, M. J., J. D. Potter, and R. J. Solaro. 1979. The calcium binding properties of phosphorylated and unphosphorylated cardiac and skeletal myosins. *J. Biol. Chem.* 254:6478–6482.

Johnson, D. E., and M. E. Cantino. 1986. High resolution biological x-ray microanalysis of diffusible ions. *In* Advanced Techniques in Biological Electron Microscopy. Springer-Verlag, Berlin. 73–100.

Kitazawa, T., H. Shuman, and A. P. Somlyo. 1982. Calcium and magnesium binding to thin and thick filaments in skinned muscle fibers: electron probe analysis. *J. Muscle Res. Cell Motil.* 3:437–454.

LeFurgey, A., M. Bond, and P. Ingram. 1988. Frontiers in electron probe X-ray microanalysis: application to cell physiology. *Ultramicroscopy*. 24:185–220.

Moss, R. L. 1992. Ca^{2+} regulation of mechanical properties of striated muscle. Mechanistic studies using extraction and replacement of regulatory proteins. *Circ. Res.* 70:865–884.

Pan, B.-S., and J. R. Solaro. 1987. Calcium-binding properties of troponin C in detergent-skinned heart muscle fibers. *J. Biol. Chem.* 262: 7839–7849.

Ridgway, E. B., and A. M. Gordon. 1984. Muscle calcium transient. Effect of post-stimulus length changes in single fibers. *J. Gen. Physiol.* 83: 75–103.

Shuman, H., A. V. Somlyo, and A. P. Somlyo. 1976. Quantitative electron probe microanalysis of biological thin sections: methods and validity. *Ultramicroscopy*. 1:317–339.

Somlyo, A. V., H. Shuman, and A. P. Somlyo. 1989. Electron probe X-ray microanalysis of Ca^{2+}, Mg^{2+}, and other ions in rapidly frozen cells. *Methods Enzymol.* 172:203–229.

Statham, P. J. 1987. Quantitative digital mapping with drift compensation. *Analytical Electron Microscopy—1987*. San Francisco Press, Inc., San Francisco. 187–190.

Trybus, K. M., and E. W. Taylor. 1980. Kinetic studies of the cooperative binding of subfragment 1 to regulated actin. *Proc. Natl. Acad. Sci. U.S.A.* 77:7209–7213.

Winegrad, S. 1965. Autoradiographic studies of intracellular calcium in frog skeletal muscle. *J. Gen. Physiol.* 48:455–479.